# Journal of Materials Chemistry A

Accepted Manuscript


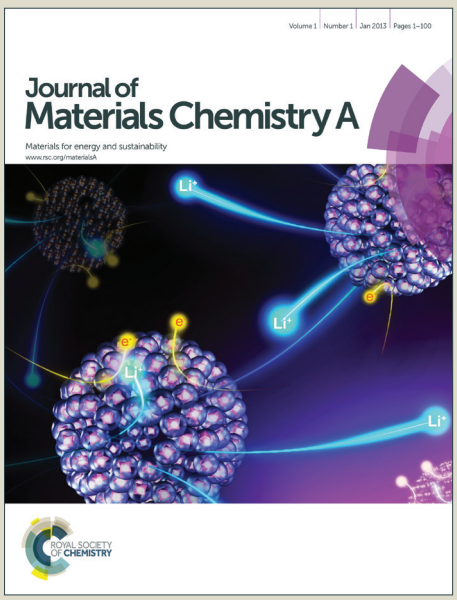





ROYAL SOCIETY OF CHEMISTRY

www.rsc.org/materialsA

# A Facile Approach to $NiCoO_2$ Intimately Standing on Nitrogen Doped Graphene Sheets by One-step hydrothermal Synthesis for Supercapacitors

Yazhou Xu[a], Junchao Wei*[a,b], Licheng Tan[a,b], Ji Yu[a], Yiwang Chen*[a,b]

[a]College of Chemistry/Institute of Polymers, Nanchang University, 999 Xuefu Avenue, Nanchang 330031, China

[b]Jiangxi Provincial Key Laboratory of New Energy Chemistry, Nanchang University, 999 Xuefu Avenue, Nanchang 330031, China

Corresponding author. Tel.: +86 791 83968703; fax: +86 791 83969561. E-mail: ywchen@ncu.edu.cn (Y. Chen); weijunchao@ncu.edu.cn (J. Wei)

**Abstract**

Novel composites based on cubic binary nickel cobaltite oxide intimately standing on nitrogen doped reduced graphene sheets (NRGO-$NiCoO_2$) were prepared by a simple one step hydrothermal synthesis. The results showed that the high crystallized $NiCoO_2$ nanoparticles with uniformly size were distributed on nitrogen-doped reduced graphene sheets (NRGO) homogeneously. The homogeneous composites combined the $NiCoO_2$ with high specific capacitance and the NRGO with the electronic conductivity, consequently low resistance conduction between metal oxides and graphenes due to barrier-free contact. The synergistic effect of NRGO substrates and $NiCoO_2$ nanoparticles promoted the electrochemical performance of the composites. The electrochemical properties of NRGO-$NiCoO_2$ can be easily tuned by altering amount of nitrogen-composed reducer. The NRGO-$NiCoO_2$ composites exhibited remarkable specific capacitance of 508 F $g^{-1}$ at 0.5 A $g^{-1}$ and excellent rate performance in cyclic voltammetry test (from 5 to 90 mV $s^{-1}$) and galvanostatic charge-discharge measurements (from 0.5 to 20 A $g^{-1}$). The capacitance maintains 93% after 2000 cycles. The flexible devices were assembled, which possess specific capacitance of 58 F $g^{-1}$ at 0.5 A $g^{-1}$. The facile one-step strategy is an effective methods for excellent supercapacitor electrodes.

**Keywords:** Pseudocapacitance; Supercapacitors; Graphene; Bi-metal Oxides

## Introduction

With the rapid development of global economy, the urgent and increasing demand for energy has greatly stimulated extensive study on energy storage devices and efficient energy harvesters.[1] Supercapacitors (SCs), also known as electrochemical capacitors or ultracapacitors, have attracted great attention from both academia and industry, because of their ultrahigh power density, excellent rate capability, fast charging/dis-charging ability, long cycle life, simple principles, easy preparation and low costs.[2-4] SCs commonly store energy based on either ion adsorption (electrochemical double layer capacitors, EDLCs) or fast surface redox reactions (pseudocapacitors).[5] The electrode materials are critical for the electrochemical performance of SCs. Pseudocapacitors materials contained conducting polymers and metal oxides, exhibit much better specific capacitance than the EDLCs materials, since the electrochemical processes occur both on the surface and in the bulk of the electrode. Therefore, metal oxides became one of the most promising materials for supercapacitors electrodes due to a better stability than that of conducting polymers.[6] A series of transition-metal oxides such as $RuO_2$,[7] $MnO_2$,[8] NiO[9-11] and $Co_3O_4$[12] have been researched. However, these transition metal oxides suffered various problems, for example high cost and toxicity. What is more, the low electronic conductivity of these transition metal oxides seriously limits their application in SCs. Compared with transition metal oxides, mixed transition metal oxides, such as $NiCo_2O_4$,[13] $CoMoO_4$,[14] and $ZnCo_2O_4$[15] combine the advantages of different metal cations and posses multiple oxidation state, leading to higher electrical conductivity and better specific capacitance. Among these different types of mixed transition metal oxides, binary nickel cobaltite oxides ($NiCo_2O_4$) has been extensively studied, due to the co-existence of Ni and Co species, which provides far-higher electrical conductivity and better redox activity than nickel oxides and cobaltite oxides.[16] Additionally, they offer many other merits such as low cost, abundant resources and environmental friendliness.[17] The $Ni^{2+}$ can replaces $Co^{2+}$ not only in the spinel $Co_3O_4$ to form the $NiCo_2O_4$, but also in the cubic crystal CoO structure to form the $NiCoO_2$.[18] So far, many works on the synthesis and electrochemical evaluation of $NiCo_2O_4$ have been

reported.[17,19] However, few works on the synthesis and electrochemical evaluation of $NiCoO_2$ are reported. In addition, the disadvantages of low electrical conductivity, aggregation easily and poor stability among the charge-discharge cycles have also limited its electrochemical performance.

Graphenes, a single layer graphite with the advantages of high specific surface area, excellent conductivity and electrochemical stability, have been studied as EDLCs for a very long time.[20,21] However, graphenes suffer some disadvantages for supercapacitors such as low specific capacitance. At the same time, graphenes tend to form irreversible agglomerates or even re-stack to form graphite through van der Waals interaction during the process of drying. To overcome these disadvantages, many work about graphenes and its composites with mixed transition metal materials have been reported. For example, $NiCo_2O_4$-graphene nanostructures were synthesized by hydrothermal and obtained a good electrochemical performance (778 F $g^{-1}$ at 1 A $g^{-1}$).[22] In addition, the mixed transition metal oxides distribute on GO surface uniformly forming GO-transition metal oxides hybrids to avoid the stack of graphenes and combine the advantages of each component.[23] Nitrogen-doped reduced graphene oxide (NRGO) has been intensively investigated as an electrode material for supercapacitors, which exhibits enhanced electrochemical performance due to the modification of the electronic structure of graphene by the N dopant.[24] Combination of nitrogen-doped graphene with mixed metal oxides is one of the effective approaches to improve the electrochemical performance of metal oxide electrode materials owing to the synergetic effect of nitrogen-doped graphenes and metal oxides. To date, N-doped graphenes can be prepared using the chemical vapor deposition (CVD) method, the arc-discharge approaches, and nitrogen plasma process. These methods require high quality equipment, strict operation conditions and incur high costs.[25] And most synthetic strategies need several steps to prepare the NRGO-$NiCoO_2$ composites.

In this study, a facile one-step hydrothermal method was proposed to fabricating ultrafine $NiCoO_2$ nanoparticles intimately standing on heterostructure nitrogen-doped reduced graphene oxide (NRGO-$NiCoO_2$) in large scale. The $NiCoO_2$ nanoparticles

were anchored on the surface of graphene tightly, and the graphene was reduced and doped with nitrogen simultaneously. The $NiCoO_2$ nanoparticles with similar particles size (20-40nm) were distributed on NRGO surface uniformly, which avoid the stack of graphene and lead to a fully utilization of $NiCoO_2$ nanoparticles to improve the specific capacitance. The favorable interfacial contact and synergistic effect between $NiCoO_2$ nanoparticles and NRGO substrates improve the electrical conductivity of NRGO-$NiCoO_2$ composites. The electrochemical performance of NRGO-$NiCoO_2$ and its flexible devices were investigated. In view of this design, the NRGO-$NiCoO_2$ composites possess an improved specific capacitance (508 F $g^{-1}$ at 0.5 A $g^{-1}$) and the capacitance maintains 93% after a 2000-cycles. The flexible devices also reveal good cycle stability with 94% capacitance remain after 2000-cycles.

## Experimental

**Synthesis of NRGO-$NiCoO_2$.** Graphene oxide (GO) was prepared from graphite powder via Hummers method and was dispersed by ultrasonication for 30 min.[26] The hybrid material of N-doped reduced graphene oxide-$NiCoO_2$ (denoted as NRGO-$NiCoO_2$) was synthesized by a hydrothermal reaction method (seen in **Scheme 1**). Firstly, 1 mmol of $Ni(NO_3)_2 \cdot 6H_2O$, and 1 mmol of $Co(NO)_2 \cdot 6H_2O$, and 15 mmol of urea were dissolved into deionized $H_2O$ (40mL), generating the intermediate complex $[M(H_2O)_{6-x}(urea)_x]^{2+}$.[27] Then 40 mL of GO (8mg/mL) and was mixed with above solution and stired for 20 min. The obtained solution was transferred into a 100 mL Teflon-lined stainless steel autoclave. Then the autoclave was heated to 200 $^oC$ and maintained for 12 h. During this process, the metal complex $[M(H_2O)_{6-x}(urea)_x]^{2+}$ began to decompose, and at the same time nitrogen doped GO (NRGO) was formed because of the presence of urea. The raw product was washed by deionized water for several times and then annealed in an atmosphere of $N_2$ at a temperature of 500 $^oC$ for 3 h. To evaluate the effect of N content on the structure and electrochemical performance of NRGO-$NiCoO_2$ composite, a series of NRGO-$NiCoO_2$ composite with different nitrogen content was prepared by tuning the amount of urea.

**Fabrication of flexible supercapacitor**: Nickel foil was first pretreated with acetone, HCl solution and deionized water to remove attached products on the surface. The electrodes were fabricated as following procedures. The 80 wt.% of as prepared NRGO-$NiCoO_2$ powders (as the active material), 10 wt.% of acetylene black (as the electrical conductor), and 10 wt.% polytetrafluoroethylene (as the binder) were mixed and milled to form a homogeneous paste. The as prepared paste was coated onto the surface of nickel foil current-collector to produce the NRGO-$NiCoO_2$ electrodes. The flexible supercapacitances were assembled using two NRGO-$NiCoO_2$ electrodes and a polypropylene membrane infiltrated KOH (3 M).

**Structural characterizations**. The morphology of different samples were characterized by environmental scanning electron microscope (SEM; FEI, QuanTA-200F), and transmission electron microscope (TEM; JEOL, JEM-2100F) with energy-dispersive X-ray spectrometry (EDS) equipment. The crystallite structures of the products were determined by X-ray diffraction (XRD; PERSEE, XD-3) with Cu Kα radiation (λ=1.5418Å) operating at 40 kV and 30 mA. The elemental compositions of the products were characterized by X-ray photoelectron spectrocopy (XPS; Thermo-VG; ESCALAB 250) with Al Kα (1,486.6 eV) X-ray source. The compositions and structure of the products were characterized by Raman spectroscopy (Raman; Horiba Jobin Yvon; XploRA microraman system) with a 523 nm of laser wavelength.

**Electrochemical measurement**. The electrochemical measurements were tested by an electrochemical working station (CHI 660E) with a typical three-electrode experimental cell at room temperature. A platinum foil and a saturated calomel electrode (SCE) were used as counter electrode and reference electrode, respectively. The cyclic voltammetry (CV), galvanostatic charge-discharge (GCD) and electrochemical impedance spectroscopy (EIS) analysis were carried out in 3 M KOH aqueous solution as the electrolyte. The specific capacitance was calculated by the following equation:

$$C_m = \frac{c}{m} = \frac{I \times \Delta t}{\Delta V \times m} \quad (1)$$

Where $C_m$ (F $g^{-1}$) is the specific capacitance, $I$ (A) is the discharge current, $\Delta t$ (s) is the discharge time, $\Delta V$ (V) is the voltage range of discharge after IR drop, and $m$ (g) is the mass of the active electrode material.

**------Scheme 1------**

**Results and Discussion**

The crystal structures of the NRGO-$NiCoO_2$ were characterized by XRD as shown in **Figure 1**. In the diffraction pattern of NRGO, two characteristic diffraction peaks appear at 25.6° and 42.9°, which are ascribed to the (002) and (100) planes of graphene sheets, respectively. Five diffraction peaks at 37.1°, 43.1°, 62.4°, 74.9° and 78.7° are observed in the XRD patterns of NRGO-$NiCoO_2$ composites, and these peaks are corresponding to the (111), (200), (220), (311) and (222) planes of cubic $NiCoO_2$, perfectly match to cubic $NiCoO_2$ (JCPDS No. 10-0188). When compared with the XRD patterns of NRGO, no crystalline peaks of NRGO are found in that of NRGO-$NiCoO_2$. This may because the surface of the NRGO in the products is covered by $NiCoO_2$ uniformly and the connection between them is very intimately, which prevent the ordered arrangement of NRGO and hinder its crystallization. The XRD patterns demonstrated that NRGO-$NiCoO_2$ cannot be formed without anneal as shown in **Figure S1**.

**------Figure 1------**

The morphologies of NRGO-$NiCoO_2$ were observed by TEM as presented in **Figure 2**. It can be seen from the low-magnification TEM images and high-magnification images of NRGO-$NiCoO_2$, the $NiCoO_2$ nanoparticles is about 20~40 nm and distribute on the NRGO substrate uniformly. Such hybrid nanostructures could provide larger contact area between electrode and electrolyte, offer extra space to store more electrolyte ions, avoid volume change of the electrode material during charge-discharge and decrease the ions' diffusion length, which are beneficial for the cycling stability of the electrode material. Furthermore, the successful growth of high-quality $NiCoO_2$ nanoparticles on the graphene is very important for the

fabrication of so-called wearable, light-weight or flexible energy-storage devices, which will find broad applications in many situations.[28] The lattice spacings of $d$ ~ 2.14 Å and 2.45 Å are shown in high resolution transmission electron microscopy (HRTEM) image of the samples, which correspond to the (200) and (111) planes of cubic $NiCoO_2$, respectively. The selected-area electron diffraction (SAED) pattern of the samples shows five obvious rings which match to the (111), (200), (220), (311), (222) planes of $NiCoO_2$, and this result is consistent with the XRD results.

**------Figure 2------**

EDS results are shown in **Figure 3a**, which indicates that the composite material contain C, N, O, Ni, Co five element. The structure details of NRGO-$NiCoO_2$ are revealed by Raman spectroscopy (**Figure 3b**). The $I_D/I_G$ intensity ratio is the indication of the degree of disorder or defects of the $sp^2$ domains.[29] For the GO substrate, there are two obvious peaks emerged at approximately 1349 $cm^{-1}$ (D band) and 1592 $cm^{-1}$ (G band). According to the results of XPS (**Figure S2** of **supplemental information**), the intensity reduction of -COOH bonding peak indicated that GO was reduced to NRGO after the hydrothermal reaction. The value of $I_D/I_G$ increases from 0.93 to 1.07, which indicates that the NRGO is more disordered then GO and the more disordered NRGO is relate to the nitrogen doped into graphene sheets. The more detailed elemental composition and the oxidation state of the as-prepared NRGO-$NiCoO_2$ are further investigated by X-ray photoelectron (XPS) measurements and the results are shown in **Figure3c-f**. By using a Gaussian fitting method, two peaks locate at 795.8 and 779.6 eV appearing in the spectrum of Co 2p, which are best fitted with the electronic states of Co $2p_{1/2}$ and Co $2p_{3/2}$, respectively.[13,30] The presence of shakeup satellite peaks (arrowed in **Figure 3c**) are ascribed to the characteristic peak of $Co^{2+}$ and $Co^{3+}$. The two peaks at binding energies of 853.6 and 872 eV appeared in the spectrum of Ni 2p, which are corresponding to the Ni $2p_{3/2}$ and Ni $2p_{1/2}$. In addition, both the satellite peaks of Ni $2p_{1/2}$ and Ni $2p_{3/2}$ (arrows in **Figure 3d**) are ascribed to the characteristic peak of $Ni^{2+}$ and $Ni^{3+}$.[31] The Ni 2p peak and Co 2p peak in the spectrum clearly indicate that the Ni and Co elements are present in the structure. The composition of NRGO-$NiCoO_2$ in the products can be

further confirmed by the O 1s peak and N 1s peak. The high-resolution spectrum for the O 1s region indicates four oxygen contributions, which have been denoted as O1 O2 O3 and O4, respectively. The peak locating at 529.1 eV (O1) is typical of metal-oxygen bonds. The well-resolved peak at 530.6 eV (O2) is always attributed to oxygen in $OH^-$ groups. The component O3 sitting at 531.8 eV is attributed to the defect sites with low oxygen coordination. The peak at 533.1 eV (O4) can be associated with multiplicity of physic- and chemi-sorbed water.[32,33] Finally the N 1s spectrum of the products shows the presence of N element. The high-resolution spectrum for N 1s region of the as-prepared NRGO-$NiCoO_2$ can be divided into three peaks, 398.2, 399.4 and 400.7 eV, which represent pyridinic N, pyrrolic N, and quaternary N, respectively.[34] All these data demonstrate that the NRGO-$NiCoO_2$ have been successfully synthesized.

To further study the affection of nitrogen amount on the structure of NRGO-$NiCoO_2$, several different NRGO-$NiCoO_2$ composites with different nitrogen content were prepared by increasing the amount of urea during the synthesis process. The XRD patterns of different NRGO-$NiCoO_2$ composites are shown in **Figure S3a**. For $NiCoO_2$ nanoparticles, the relative intensity of diffraction peaks reduces with the increasing of nitrogen amount. Nevertheless, for NRGO, the relative intensity of diffraction peaks increase with the increasing of nitrogen amount. The partial enlargement details are shown in the inset of **Figure S3a**. The results indicate that the increased degree of reduction of NRGO with the addition of nitrogen amount to result in a much ordered arrangement, which show a higher diffraction peak at the 2 theta of $26^o$. As can be seen in **Figure S3b**, the addition of 54 wt.% urea is the critical value. Cubic $NiCoO_2$ was not obtained while the excessive amount of urea. Besides, the cubic $NiCoO_2$ was unable to form when ascorbic acid was used as reducing agent, although the reducibility of ascorbic acid is better than urea. Moreover, mechanical stirring was unfavorable to formation of cubic $NiCoO_2$ as shown in **Figure S3c**. **Figure S3d** shows the Raman spectroscopy of different NRGO-$NiCoO_2$ composites with increased nitrogen amount. The $I_D/I_G$ intensity ratio are 1.02 (42 wt.%), 1.04 (48 wt.%) and 1.07 (54 wt.%), respectively, which indicate that the disorder of NRGO

substrate increases with the increasing of nitrogen amount. The increasing disorder of NRGO is caused by the increasing level of nitrogen doping. The nitrogen content of NRGO-$NiCoO_2$ composites were confirmed by XPS as shown in **Figure S3e**. The nitrogen content are 0.79%, 1.24% and 1.43% for 42 wt.%, 48 wt.% and 54 wt.% urea addition, respectively.

**------Figure 3------**

Cyclic voltammetry and galvanostatic charge-discharge curves were obtained in a three-electrode cell to evaluate the electrochemical properties of the pure $NiCoO_2$ nanoparticles and NRGO-$NiCoO_2$ composite material. **Figure 4a** shows the typical CV curves with the scan rate of 50 mV $s^{-1}$. The CV curves of NRGO-$NiCoO_2$ show a pair of obvious redox peaks, while no significant redox peaks are observed in the CV curves of pure $NiCoO_2$ nanoparticles. Besides, the integral area of CV curves of NRGO-$NiCoO_2$ is far greater than that of $NiCoO_2$ nanoparticles, indicating that pure $NiCoO_2$ nanoparticles aggregate easily and can hardly take part in redox reaction efficiently. As for NRGO-$NiCoO_2$, dispersion of $NiCoO_2$ nanoparticles on the surface of NRGO homogeneously is beneficial to all the $NiCoO_2$ nanoparticles involving in redox reaction easily. In addition, the uniformly distribution of $NiCoO_2$ nanoparticles can also improve the specific capacitance of NRGO-$NiCoO_2$, and these results are corresponding to the TEM figures. **Figure 4b** presents the GCD curves of pure $NiCoO_2$ and NRGO-$NiCoO_2$ composites at a current density of 1 A $g^{-1}$. The longer discharge time indicates a larger specific capacitance, which due to the larger surface of NRGO and the $NiCoO_2$ nanoparticles on the surface of NRGO substrate. **Figure 4c** shows the relationships of specific capacitance with the current density of pure $NiCoO_2$ nanoparticles and NRGO-$NiCoO_2$ composites. The specific capacitance of NRGO-$NiCoO_2$ composites is quintuple that of $NiCoO_2$ nanoparticles at the current density of 1 A $g^{-1}$. When the current density increase to 20 A $g^{-1}$, the specific capacitance of NRGO-$NiCoO_2$ composite material is still quadruple that of $NiCoO_2$ nanoparticles.

The EIS analysis is generally used to evaluate the behavior of electrochemical capacitor, and to decide the parameters affecting the performance of an electrode. The

Nyquist plots of NRGO-$NiCoO_2$ composites are shown in **Figure 4d**. The equivalent electrical circuit consists is shown in the inset of **Figure 4d**. A semicircle at high frequency and a straight line at low frequency are observed in this figure. The point of intersection with the real impedance axis is the solution resistance ($R_s$) which include the measurement of the electrolyte ohmic resistance, the intrinsic resistance of electrode material and contact resistance of the interface of electrode materials and current collector.[35] The semicircle in the high frequency range represents the charge-transfer resistance ($R_{ct}$), which occurring on the surface of electrode and electrolyte during the electrochemical reaction.[36] The straight line followed with semicircle is the Warburg impedance ($Z_w$) which represents a kinetic of the diffusion process caused by diffusion of electrolyte ions occurring in electrodes. The $R_s$ values of $NiCoO_2$ nanoparticles and NRGO-$NiCoO_2$ composite materials are 0.7 ohm and 0.81 ohm, respectively. The tiny difference and low values of $R_s$ indicate that both the conductivity of NRGO-$NiCoO_2$ composites and the electrical contact between NRGO-$NiCoO_2$ composites and current collector are very excellent. The $R_{ct}$ value of NRGO-$NiCoO_2$ composite materials is 0.44 ohm, which is smaller than that of $NiCoO_2$ nanoparticles (0.61 ohm). The low $R_{ct}$ values are associated with the excellent charge-transfer rate between electrode and electrolyte. The lower $R_{ct}$ value of NRGO-$NiCoO_2$ composite materials than $NiCoO_2$ nanoparticles is caused by the introduction of NRGO substrates. It is the NRGO that promotes the electron conductivity of NRGO-$NiCoO_2$ composite materials. The line with a slope indicates the Warburg behavior. For an ideal supercapacitor, the Nyqusit plot should be a vertical line at low frequency, which parallel to the imaginary impedance axis. Compared with pure $NiCoO_2$ nanoparticles, the steeper line of NRGO-$NiCoO_2$ composites is much closer to the ideal behavior which demonstrates a faster kinetics of diffusion process. The improved performance of electrical conductivity is attributed to the synergistic effect between NRGO and $NiCoO_2$ nanoparticles.[35,37] The non-ideality lines followed with semicircle are associated with constant phase element (CPE). The CPE of NRGO-$NiCoO_2$ composites is caused by rough surface of NRGO-$NiCoO_2$ and inhomogeneous distribution of active sites.

**------Figure 4------**

To study the affection of different nitrogen amount to the electrochemical performances of NRGO-$NiCoO_2$ composites, several samples with increasing weight rate of urea were evaluated through cyclic voltammetry, and galvanostatic charge-discharge and electrochemical impedance spectroscopy test respectively. **Figure 5a** shows the typical CV curves of NRGO-$NiCoO_2$ composites (with the scan rate of 20 mV $s^{-1}$) with increasing nitrogen amount. Compared with the pure $NiCoO_2$ nanoparticles, the NRGO-$NiCoO_2$ composite material with increasing degree of nitrogen doping shows a pair of obvious redox peaks which indicates pseudocapacitance effect. Besides, the integral area of NRGO-$NiCoO_2$ increases with the increasing of nitrogen amount, which indicates that the specific capacitance of NRGO-$NiCoO_2$ composite materials increases with the increasing nitrogen amount. **Figure 5b** presents the GCD curves of NRGO-$NiCoO_2$ composites with increasing nitrogen amount at a current density of 1 A $g^{-1}$. The discharge time of NRGO-$NiCoO_2$ increases with the increasing of nitrogen amount which indicates that the specific capacitance also gradually increases. **Figure 5c** shows the specific capacitance of NRGO-$NiCoO_2$ composites with different nitrogen amount at different current densities from 0.5 A $g^{-1}$ to 20 A $g^{-1}$. The specific capacitance of NRGO-$NiCoO_2$ composites (based on GCD) increases with the increasing of nitrogen amount. In addition, the specific capacitance at a current density of 20 A $g^{-1}$ (320 F $g^{-1}$) still maintain nearly 65% compared with the value at 0.5 A $g^{-1}$ (490 F $g^{-1}$). The high specific capacitance of NRGO-$NiCoO_2$ composites with 54 wt.% urea at high current density can be attributed to following factors: (1) The NRGO substrates with hybrid structure improve the effective specific surface area and reduce the ion-diffusion route. (2) The doping of N atom provides pseudocapacitance and improves wettability of electrode/electrolyte surface. (3) The intimate connection between NRGO and $NiCoO_2$ promotes the electrical conductivity.[38-41] The Nyquist plots of NRGO-$NiCoO_2$ composites with different weight rate of urea are shown in **Figure 5d**. Four lines with a slope are observed, which indicates the Warburg behavior. The slope of lines increases with the increasing of nitrogen amount which demonstrates that the

impedance of samples reduces with the increasing of nitrogen amount. The reason may be attributed to the following factors: (1) The N-doped graphene promotes the diffusion of electrolyte ions. (2) The degree of reduction of NRGO becomes higher with the increasing of nitrogen amount which promotes the electric conductivity. (3) The barrier-free contact of NRGO substrates and $NiCoO_2$ nanoparticles reduces the contact resistance of the composites significantly. (4) The modification of GO with N atom introduces pseudocapacitance. The N-dopers act as electron donor to promote charge density of the space charge layer, consequently strengthening the electric conductivity.[42]

**------Figure 5------**

To evaluate the details of electrochemical performance for NRGO-$NiCoO_2$ composites, **Figure 6a** shows the typical CV curves of NRGO-$NiCoO_2$ electrode material in a 3 M KOH aqueous electrolyte at various scan rates ranging from 5 to 90 mV $s^{-1}$. A pair of redox peaks appeared within the potential range from 0 V to 0.5 V vs. SCE for all sweep rates, which indicates that the NRGO-$NiCoO_2$ can work efficiently as pseudocapacitor electrodes. This pair of peaks is mainly due to M-O/M-O-OH (M represents Ni or Co).[43] The high-power characteristic of the NRGO-$NiCoO_2$ electrode can be testified from the voltammetric response at different scan rates. All curves show a similar shape, and the current density increase with the increasing scan rate. Even at a high scan rate of 90 mV $s^{-1}$, the CV curve still shows a pair of redox peaks, which indicate that this kind of structure is beneficial to fast redox reactions and the excellent contact improves the stability of NRGO-$NiCoO_2$ composites leading to well maintain of specific capacitance.[13] In addition, with the increasing of the scan rate, the reduction peaks shift to a more negative position, while oxidation peak hardly shift to a more positive position, which indicate that the internal diffusion resistance basically maintains the same level with the increasing scan rate.[36] GCD tests were implemented in 3 M KOH electrolyte between 0V to 0.5V (vs. SCE). **Figure 6b** shows galvanostatic discharge curves of the NRGO-$NiCoO_2$ samples at different currents densities from 0.5 A $g^{-1}$ to 20 A $g^{-1}$. The typical galvanostatic charge-discharge curves at the current density of 5 A $g^{-1}$ is listed in the inset of **Figure 6b**, and the results

suggest that the voltage plateaus of the electrode is accordant with the peaks observed in CV curves. The internal resistance drop (IR drop) is mainly resulted from the current of the bulk electrode.[44] The average specific capacitance of NRGO-$NiCoO_2$ can be calculated from the galvanostatic charge-discharge curves as shown in **Figure 6c**. The NRGO-$NiCoO_2$ possess specific capacitance of 508, 490, 386, 270, 216, 156 F $g^{-1}$ at the discharge currents of 0.5, 1, 2, 5, 10, 20 A $g^{-1}$, respectively. Due to the decreasing utilization of active materials cased by the increased diffusion of ions, the specific capacitance decreases with the increasing of the current density.[45] The cycle stability of the NRGO-$NiCoO_2$ composite is demonstrated in **Figure 6d**. At the first 200 cycles, the specific capacitance of the sample decreases. During the beginning process, the NRGO-$NiCoO_2$ composites are completely activated through the intercalation and de-intercalation of electrolyte ions and lead to the increase of active points of the electrodes, thus improving the specific capacitance. After a 2000 cycle test, the specific capacitance maintains 93% of total specific capacitance. The integrated galvanostatic charge-discharge curves at current density of 2 A $g^{-1}$ from 80000 sec. to 81000 sec. in the inset of **Figure 6d** indicate that the columbic efficiency is nearly 100% during this period. The outstanding cycling stability of NRGO-$NiCoO_2$ composites can be attributed to the excellent connection between NRGO and $NiCoO_2$. $NiCoO_2$ nanoparticles standing on GO nanosheets intimately lead to barrier-free contact, which decrease internal resistance effectivity.

**------Figure 6------**

To further explore the electrochemical performance of NRGO-$NiCoO_2$ composites in flexible electronic devices. The flexible supercapacitors were assembled using two pieces of NRGO-$NiCoO_2$ composite coating on nickel foil as electrodes and a polypropylene membrane infiltrated KOH (3 M) as separator. The electrochemical performance of flexible device were tested by an electrochemical working station (CHI 660E) with a typical two-electrode experimental cell. The flexible device can be bent from flat to radius (shown in **Figure 7a**). **Figure 7b** shows the CV curves of the flexible device between 0 and 0.8 V at different scan rates in the range from 5 to 90 mV $s^{-1}$. A rectangular-like shape of the CV curves indicates an ideal capacitor

behavior. To evaluate the electrochemical performance as flexible energy storage device, the CV of flexible device under various bending angle (ranging from $0^o$ to $180^o$) were performed. As shown in **Figure 7c**, the flexible device shows stable behavior and completely recoverable properties. It can be seen from **Figure 7b** and **7c**, the CV curves of two electrode system are quite different from those of three electrode system, because of the absence of redox peaks. The reasons are as follows: the mechanisms of electrical double-layer capacitor and faradic redox pseudocapacitors can work separately or together. For the two electrode system, it indicates that the mechanisms of double-layer capacitor occupied dominant. In addition, no obvious redox peaks observed in the CV curves of two electrode system reveals that the current supercapacitors are cycling at a pseudocanstant rate.[46] The as prepared flexible device exhibits good long-term cycling stability performance. **Figure 7d** shows the GCD curves of the flexible device at various current densitys from 0.5 A $g^{-1}$ to 10 A $g^{-1}$. The specific capacitance of flexible devices can be calculated from the GCD curves in **Figure 7d**, and the results are shown in **Figure 7e**. The flexible devices show capacitance of 58, 51, 48, 45, 41 F $g^{-1}$ at the discharge currents of 0.5, 1, 2, 5, 10 A $g^{-1}$, respectively, showing a good rate-performance. **Figure 7f** demonstrates that a red light-emitting diode (LED) can be light by the NRGO-$NiCoO_2$ composite flexible devices.

**------Figure 7------**

**Figure 8a** shows the cycling stability test in the range of 0 to 0.8 V at a current density of 1 A $g^{-1}$. After 2000 cycles, the specific capacitance still maintain 94%, indicating that the flexible device own stable good cycling performance. The remarkable electrochemical performance can be attributed to NRGO-$NiCoO_2$ composites forming a good interpenetrating structure between electrode and electrolyte. EIS tests are carried out to further understand the electrochemical behavior of the flexible devices. The Nyquist plots of the flexible devices before and after 2000 cycles are shown in **Figure 8b**. Obviously, the EIS plots are similar. The value of equivalent series resistant obtained for the flexible devices before and after 2000 cycles are 0.25 Ω, which indicates that the as-prepared flexible devices possess

excellent stability. The cycle stability of the flexible devices was evaluated by CV test at a scan rate of 50 mV $s^{-1}$ for 2000 cycles again (shown in **Figure 8c**). A rectangular-like shape of the CV curves before and after 2000 cycles are basic coincidence with the almost same integral area, indicating that the specific capacitances of the flexible devices before and after 2000 cycles keep unchanged. EIS tests were also used to evaluating the electrochemical behavior of the flexible devices. Both the value of equivalent series resistant before and after 2000 cycles are 0.26 Ω. Besides, the EIS plots are maintained after 2000 cycles, revealing that the flexible devices have excellent stability. The low internal resistance and remarkable cycling stability can be attributed to the synergistic effect of NRGO nanosheets and $NiCoO_2$ nanoparticles, uniform distribution of $NiCoO_2$ nanoparticles on NRGO nanosheets and barrier-free contact between $NiCoO_2$ nanoparticles and NRGO nanosheets.

**------Figure 8------**

## 4. Conclusions

In summary, a facile process was developed to synthesis $NiCoO_2$ nanoparticles and its nitrogen doped reduced graphene oxide based composites by one step hydrothermal synthesis. Through this strategy, GO was doped by N atom with accompanying by reduction of GO to form NRGO. At the same time, $NiCoO_2$ nanoparticles were anchored on NRGO substrates intimately leading to barrier-free contact. The electrochemical performance of NRGO-$NiCoO_2$ composites were evaluated and the potential applications in flexible devices were also been fabricated successfully. The NRGO-$NiCoO_2$ composites as electrode materials show the remarkable electrochemical performance with a specific capacitance of 509 F $g^{-1}$ at a current density of 0.5 A $g^{-1}$ according to the GCD tests. In addition, the NRGO-$NiCoO_2$ composites exhibit good cyclic stability which maintains 93% after 2000 charge-discharge cycles. The excellent value of specific capacitance along with reasonable cycling stability makes the NRGO-$NiCoO_2$ composites as promising candidate electrodes for fabricating flexible energy storage devices.

## Supporting information

High-resolution XPS spectra of C 1s for GO and NRGO. XRD pattern of the $NiCoO_2$ -NRGO composites with various nitrogen amount and through different methods. Raman spectra of $NiCoO_2$ -NRGO composites with various nitrogen amount. This information is available free of charge via the Internet at http://pubs.rsc.org.

**Acknowledgements**

This work was financially supported by the National Natural Science Foundation of China (51203073 and 51463013), National Science Fund for Distinguished Young Scholars (51425304), and the Natural Science Foundation of Jiangxi Province (No. 2142BAB203018). Yazhou Xu and Junchao Wei contributed equally to this work.

**References**

(1) Sharma, R.; Bufon, C. C. B.; Grimm, D.; Sommer, R.; Wollatz, A.; Schadewald, J.; Thurmer, D. J.; Siles, P. F.; Bauer, M.; Schmidt, O. G. Large-Area Rolled-Up Nanomembrane Capacitor Arrays for Electrostatic Energy Storage. *Adv. Energy Mater.* **2014**, *4*, DOI:10.1002/aenm.201301631.

(2) Yan, J.; Wang, Q.; Wei, T.; Fan, Z. Recent Advances in Design and Fabrication of Electrochemical Supercapacitors with High Energy Densities. *Adv. Energy Mater.* **2014**, *4*, DOI:10.1002/aenm.201300816.

(3) Zhang, L. L.; Zhao, X. S. Carbon-Based Materials as Supercapacitor Electrodes. *Chem. Soc. Rev.* **2009**, *38*, 2520-2531.

(4) Liu, C.; Li, F.; Ma, L. P.; Cheng, H.-M. Advanced Materials for Energy Storage. *Adv. Mater.* **2010**, *22*, E28-E62.

(5) Simon, P.; Gogotsi, Y. Materials for Electrochemical Capacitors. *Nat. Mater.* **2008**, *7*, 845-854.

(6) Wang, G.; Zhang, L.; Zhang, J. A Review of Electrode Materials for Electrochemical Supercapacitors. *Chem. Soc. Rev.* **2012**, *41*, 797-828.

(7) Sugimoto, W.; Iwata, H.; Yasunaga, Y.; Murakami, Y.; Takasu, Y. Preparation of Ruthenic Acid Nanosheets and Utilization of Its Interlayer Surface for

Electrochemical Energy Storage. *Angew. Chem. Int. Ed.* **2003**, *42*, 4092-4096.

(8) Yan, J.; Khoo, E.; Sumboja, A.; Lee, P. S. Facile Coating of Manganese Oxide on Tin Oxide Nanowires with High-Performance Capacitive Behavior. *ACS Nano* **2010**, *4*, 4247-4255.

(9) Xia, X. H.; Tu, J. P.; Wang, X. L.; Gu, C. D.; Zhao, X. B. Hierarchically Porous NiO Film Grown by Chemical Bath Deposition via a Colloidal Crystal Template as An Electrochemical Pseudocapacitor Material. *J. Mater. Chem.* **2011**, *21*, 671-679.

(10) Feng, X.; Chen, N.; Zhang, Y.; Yan, Z.; Liu, X.; Ma, Y.; Shen, Q.; Wang, L.; Huang, W. The Self-Assembly of Shape Controlled Functionalized Graphene–$MnO_2$ Composites for Application as Supercapacitors. *J. Mater. Chem. A* **2014**, *2*, 9178-9184.

(11) Feng, X.; Yan, Z.; Chen, N.; Zhang, Y.; Ma, Y.; Liu, X.; Fan, Q.; Wang, L.; Huang, W. The Synthesis of Shape-Controlled $MnO_2$/Graphene Composites via a Facile One-Step Hydrothermal Method and Their Application in Supercapacitors *J. Mater. Chem. A* **2013**, *1*, 12818-12825.

(12) Wei, T. Y.; Chen, C. H.; Chang, K. H.; Lu, S. Y.; Hu, C. C. Cobalt Oxide Aerogels of Ideal Supercapacitive Properties Prepared with an Epoxide Synthetic Route. *Chem. Mater.* **2009**, *21*, 3228-3233.

(13) Yuan, C.; Li, J.; Hou, L.; Zhang, X.; Shen, L.; Lou, X. W. D. Ultrathin Mesoporous $NiCo_2O_4$ Nanosheets Supported on Ni Foam as Advanced Electrodes for Supercapacitors. *Adv. Funct. Mater.* **2012**, *22*, 4592-4597.

(14) Liu, M. C.; Kong, L. B.; Lu, C.; Ma, X. J.; Li, X. M.; Luo, Y. C.; Kang, L. Design and Synthesis of $CoMoO_4$-$NiMoO_4 \cdot xH_2O$ Bundles with Improved Electrochemical Properties for Supercapacitors. *J. Mater. Chem. A* **2013**, *1*, 1380-1387.

(15) Liu, B.; Liu, B.; Wang, Q.; Wang, X.; Xiang, Q.; Chen, D.; Shen, G. New Energy Storage Option: Toward $ZnCo_2O_4$ Nanorods/Nickel Foam Architectures for High-Performance Supercapacitors. *ACS Appl. Mater. Interfaces* **2013**, *5*, 10011-10017.

(16) Zhang, G. Q.; Wu, H. B.; Hoster, H. E.; Chan-Park, M. B.; Lou, X. W. Single-Crystalline $NiCo_2O_4$ Nanoneedle Arrays Grown on Conductive Substrates as Binder-Free Electrodes for High-Performance Supercapacitors. *Energy Environ. Sci.* **2012**, *5*, 9453-9456.

(17) Jiang, H.; Ma, J.; Li, C. Hierarchical Porous $NiCo_2O_4$ Nanowires for High-Rate Supercapacitors. *Chem. Commun.* **2012**, *48*, 4465-4467.

(18) Xiao, J.; Yang, S. Bio-Inspired Synthesis of NaCl-type $Co_xNi_{1-x}O$ ($0 \leq x < 1$) Nanorods on Reduced Graphene Oxide Sheets and Screening for Asymmetric Electrochemical Capacitors. *J. Mater. Chem.* **2012**, *22*, 12253-12262.

(19) Wei, T. Y.; Chen, C. H.; Chien, H. C.; Lu, S. Y.; Hu, C. C. A Cost-Effective Supercapacitor Material of Ultrahigh Specific Capacitances: Spinel Nickel Cobaltite Aerogels from an Epoxide-Driven Sol-Gel Process. *Adv. Mater.* **2010**, *22*, 347-351.

(20) Sun, Y.; Wu, Q.; Shi, G. Graphene Based New Energy Materials. *Energy Environ. Sci.* **2011**, *4*, 1113-1132.

(21) Zhai, Y.; Dou, Y.; Zhao, D.; Fulvio, P. F.; Mayes, R. T.; Dai, S. Carbon Materials for Chemical Capacitive Energy Storage. *Adv. Mater.* **2011**, *23*, 4828-4850.

(22) Wei, Y.; Chen, S.; Su, D.; Sun, B.; Zhu, J.; Wang, G. 3D Mesoporous Hybrid $NiCo_2O_4$@Graphene Nanoarchitectures as Electrode Materials for Supercapacitors with Enhanced Performances. *J. Mater. Chem. A* **2014**, *2*, 8103-8109.

(23) Mai, Y.; Zhang, F.; Feng, X. Polymer-directed Synthesis of Metal Oxide-Containing Nanomaterials for Electrochemical Energy Storage. *Nanoscale* **2014**, *6*, 106-121.

(24) Han, J.; Zhang, L. L.; Lee, S.; Oh, J.; Lee, K. S.; Potts, J. R.; Ji, J.; Zhao, X.; Ruoff, R. S.; Park, S. Generation of B□Doped Graphene Nanoplatelets Using a Solution Process and Their Supercapacitor Applications. *ACS Nano* **2012**, *7*, 19-26.

(25) Fan, W.; Xia, Y. Y.; Tjiu, W. W.; Pallathadka, P. K.; He, C.; Liu, T. Nitrogen-Doped Graphene Hollow Nanospheres as Novel Electrode Materials for Supercapacitor Applications. *J. Power Sources* **2013**, *243*, 973-981.

(26) Hummers, W. S.; Offeman, R. E. Preparation of Graphitic Oxide. *J. Am. Chem. Soc.* **1958**, *80*, 1339-1339.

(27) Chen, S.; Qiao, S. Z. Hierarchically Porous Nitrogen-Doped Graphene-$NiCo_2O_4$ Hybrid Paper as an Advanced Electrocatalytic Water-Splitting Material. *ACS Nano* **2013**, *7*, 10190-10196.

(28) Zhang, G.; Lou, X. W. General Solution Growth of Mesoporous $NiCo_2O_4$ Nanosheets on Various Conductive Substrates as High-Performance Electrodes for Supercapacitors. *Adv. Mater.* **2013**, *25*, 976-979.

(29) Choi, C. H.; Park, S. H.; Woo, S. I. Binary and Ternary Doping of Nitrogen, Boron, and Phosphorus into Carbon for Enhancing Electrochemical Oxygen Reduction Activity. *ACS Nano* **2012**, *6*, 7084-7091.

(30) Cui, B.; Lin, H.; Liu, Y. Z.; Li, J. B.; Sun, P.; Zhao, X. C.; Liu, C. J. Photophysical and Photocatalytic Properties of Core-Ring Structured $NiCo_2O_4$ Nanoplatelets. *J. Phys. Chem. C* **2009**, *113*, 14083-14087.

(31) Peck, M. A.; Langell, M. A. Comparison of Nanoscaled and Bulk NiO Structural and Environmental Characteristics by XRD, XAFS, and XPS. *Chem. Mater.* **2012**, *24*, 4483-4490.

(32) Marco, J. F.; Gancedo, J. R.; Gracia, M.; Gautier, J. L.; Ríos, E.; Berry, F. J. Characterization of the Nickel Cobaltite, $NiCo_2O_4$, Prepared by Several Methods: An XRD, XANES, EXAFS, and XPS Study. *J. Solid State Chem.* **2000**, *153*, 74-81.

(33) Jiménez, V. M.; Fernández, A.; Espinós, J. P.; González-Elipe, A. R. The State of the Oxygen at the Surface of Polycrystalline Cobalt Oxide. *J. Electron Spectrosc. Rel. Phen.* **1995**, *71*, 61-71.

(34) Jeong, H. M.; Lee, J. W.; Shin, W. H.; Choi, Y. J.; Shin, H. J.; Kang, J. K.; Choi, J. W. Nitrogen-Doped Graphene for High-Performance Ultracapacitors and the Importance of Nitrogen-Doped Sites at Basal Planes. *Nano Lett.* **2011**, *11*, 2472-2477.

(35) Ghosh, D.; Giri, S.; Das, C. K. Synthesis, Characterization and Electrochemical Performance of Graphene Decorated with 1D $NiMoO_4 \cdot nH_2O$ Nanorods. *Nanoscale* **2013**, *5*, 10428-10437.

(36) Li, L.; Xu, J.; Lei, J.; Zhang, J.; McLarnon, F.; Wei, Z.; Li, N.; Pan, F. A One-Step, Cost-Effective Green Method to in situ Fabricate $Ni(OH)_2$ Hexagonal Platelets on Ni Foam as Binder-Free Supercapacitor Electrode Materials. *J. Mater.*

*Chem. A* **2015**, DOI:10.1039/C4TA05156D.

(37) Bello, A.; Makgopa, K.; Fabiane, M.; Dodoo-Ahrin, D.; Ozoemena, K. I.; Manyala, N. Chemical Adsorption of NiO Nanostructures on Nickel Foam-Graphene for Supercapacitor Applications. *J. Mater. Sci.* **2013**, *48*, 6707-6712.

(38) Hulicova, D.; Kodama, M.; Hatori, H. Electrochemical Performance of Nitrogen-Enriched Carbons in Aqueous and Non-Aqueous Supercapacitors. *Chem. Mater.* **2006**, *18*, 2318-2326.

(39) Hulicova-Jurcakova, D.; Kodama, M.; Shiraishi, S.; Hatori, H.; Zhu, Z. H.; Lu, G. Q. Nitrogen-Enriched Nonporous Carbon Electrodes with Extraordinary Supercapacitance. *Adv. Funct. Mater.* **2009**, *19*, 1800-1809.

(40) Wang, D. W.; Li, F.; Yin, L. C.; Lu, X.; Chen, Z. G.; Gentle, I. R.; Lu, G. Q.; Cheng, H.-M. Nitrogen-Doped Carbon Monolith for Alkaline Supercapacitors and Understanding Nitrogen-Induced Redox Transitions. *Chem. Eur. J.* **2012**, *18*, 5345-5351.

(41) Ma, F.; Zhao, H.; Sun, L.; Li, Q.; Huo, L.; Xia, T.; Gao, S.; Pang, G.; Shi, Z.; Feng, S. A facile Route for Nitrogen-Doped Hollow Graphitic Carbon Spheres with Superior Performance in Supercapacitors. *J. Mater. Chem.* **2012**, *22*, 13464-13468.

(42) Su, F.; Poh, C. K.; Chen, J. S.; Xu, G.; Wang, D.; Li, Q.; Lin, J.; Lou, X. W. Nitrogen-Containing Microporous Carbon Nanospheres with Improved Capacitive Properties. *Energy Environ. Sci.* **2011**, *4*, 717-724.

(43) Wang, H.; Gao, Q.; Jiang, L. Facile Approach to Prepare Nickel Cobaltite Nanowire Materials for Supercapacitors. *Small* **2011**, *7*, 2454-2459.

(44) Kang, J.; Hirata, A.; Qiu, H. J.; Chen, L.; Ge, X.; Fujita, T.; Chen, M. Self-Grown Oxy-Hydroxide@ Nanoporous Metal Electrode for High-Performance Supercapacitors. *Adv. Mater.* **2014**, *26*, 269-272.

(45) Zhang, G.; Li, W.; Xie, K.; Yu, F.; Huang, H. A One-Step and Binder-Free Method to Fabricate Hierarchical Nickel-Based Supercapacitor Electrodes with Excellent Performance. *Adv. Funct. Mater.* **2013**, *23*, 3675-3681.

(46) Yang, L.; Cheng, S.; Ding, Y.; Zhu, X.; Wang, Z. L.; Liu, M. Hierarchical Network Architectures of Carbon Fiber Paper Supported Cobalt Oxide Nanonet for

High-Capacity Pseudocapacitors. *Nano Lett.* **2011**, *12*, 321-325.

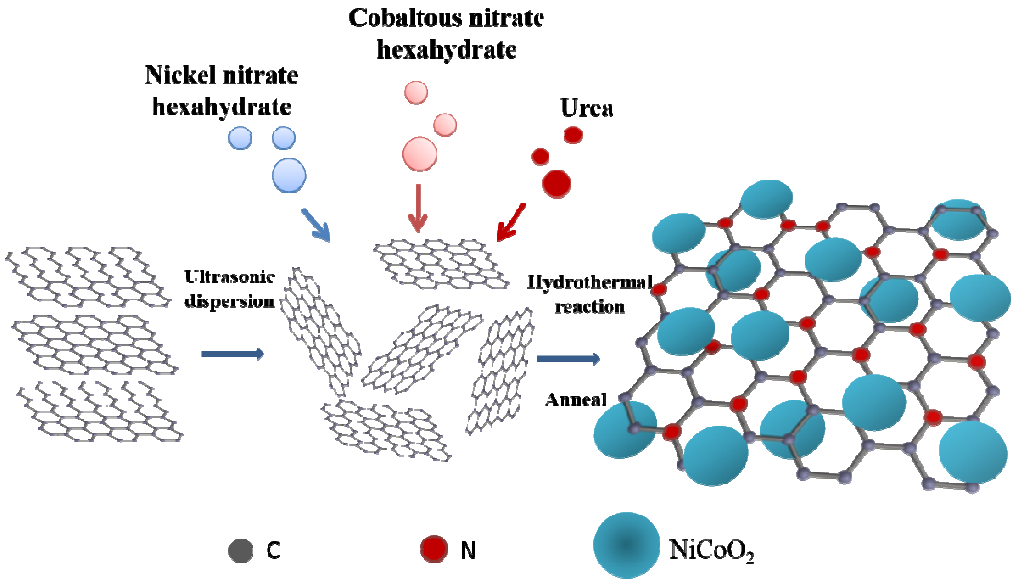


**Scheme 1.** Schematic illustration for the formation processes of the $NiCoO_2$ nanoparticles on NRGO substrate.

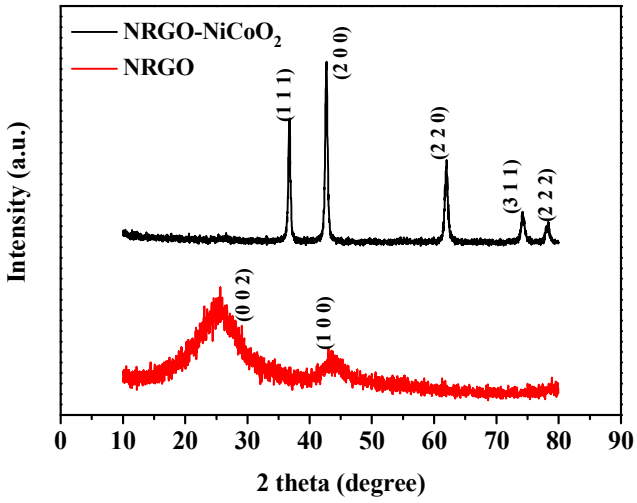


**Figure 1**. XRD pattern of the $NiCoO_2$-NRGO composites.

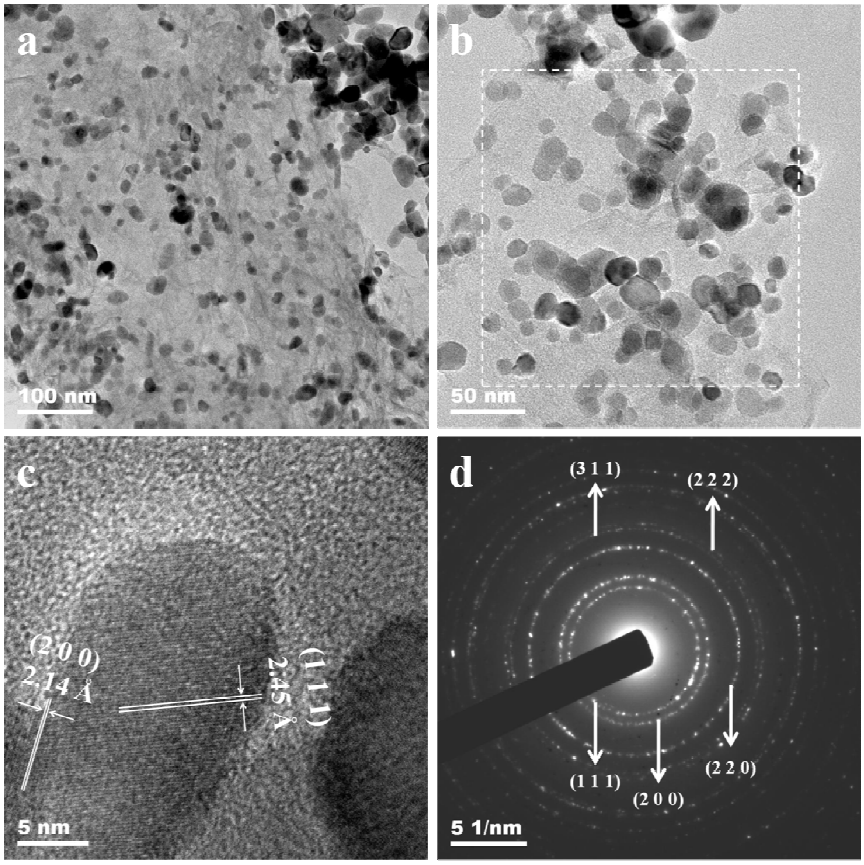


**Figure 2.** (a) Low-magnification TEM image, (b) high-magnification TEM image, (c) HRTEM image, (d) SAED pattern of NRGO-$NiCoO_2$ composite materials.

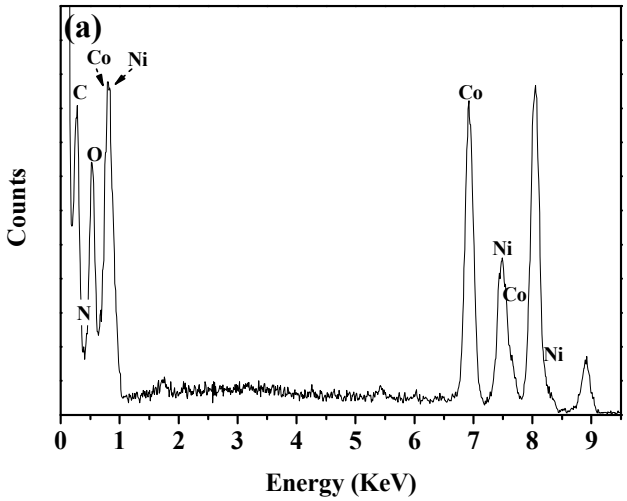


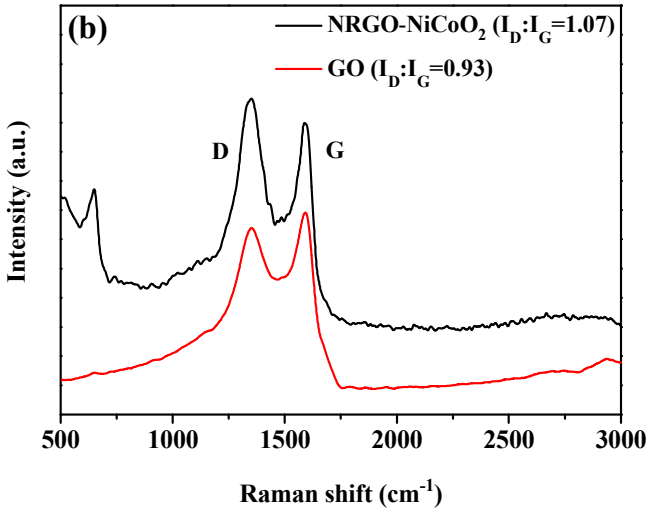

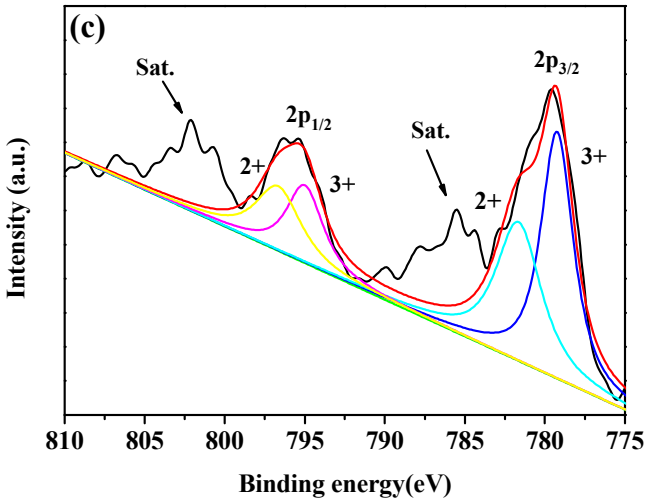


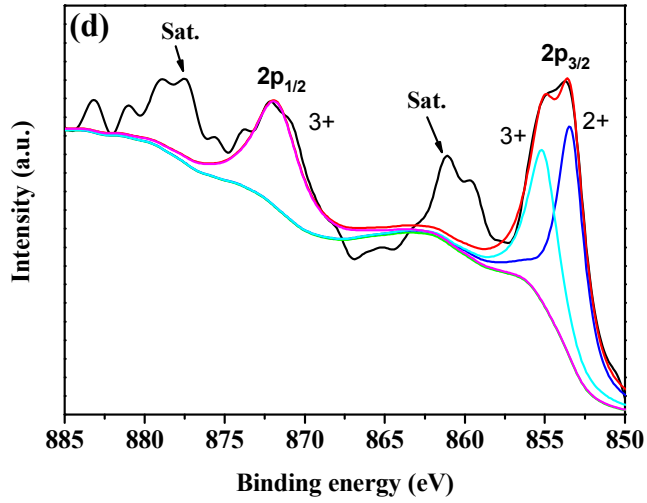

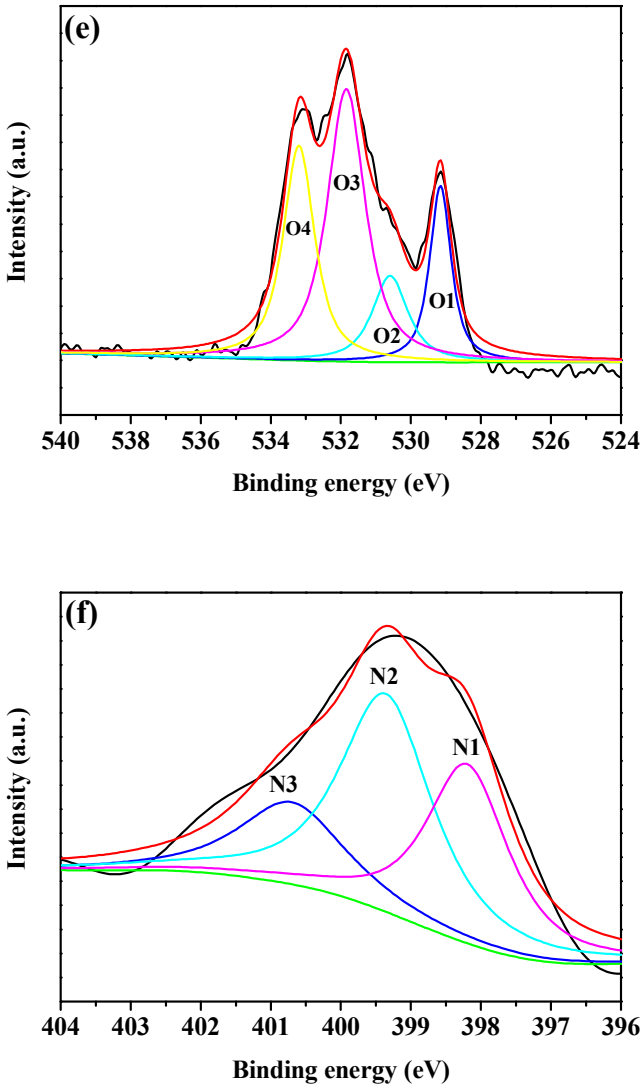


**Figure 3.** (a) EDS image of NRGO-$NiCoO_2$ composites, (b) Raman spectra of NRGO-$NiCoO_2$ and GO, High-resolution XPS spectra of (c) Co 2p, (d) Ni 2p, (e) O 1s, (f) N 1s for NRGO-$NiCoO_2$ composites.

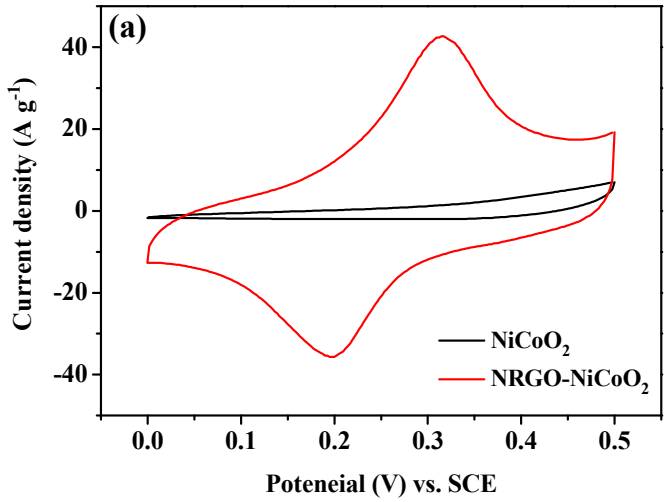


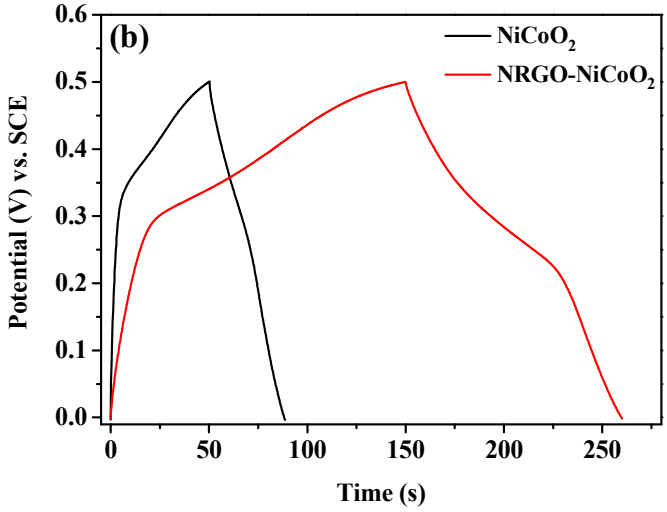

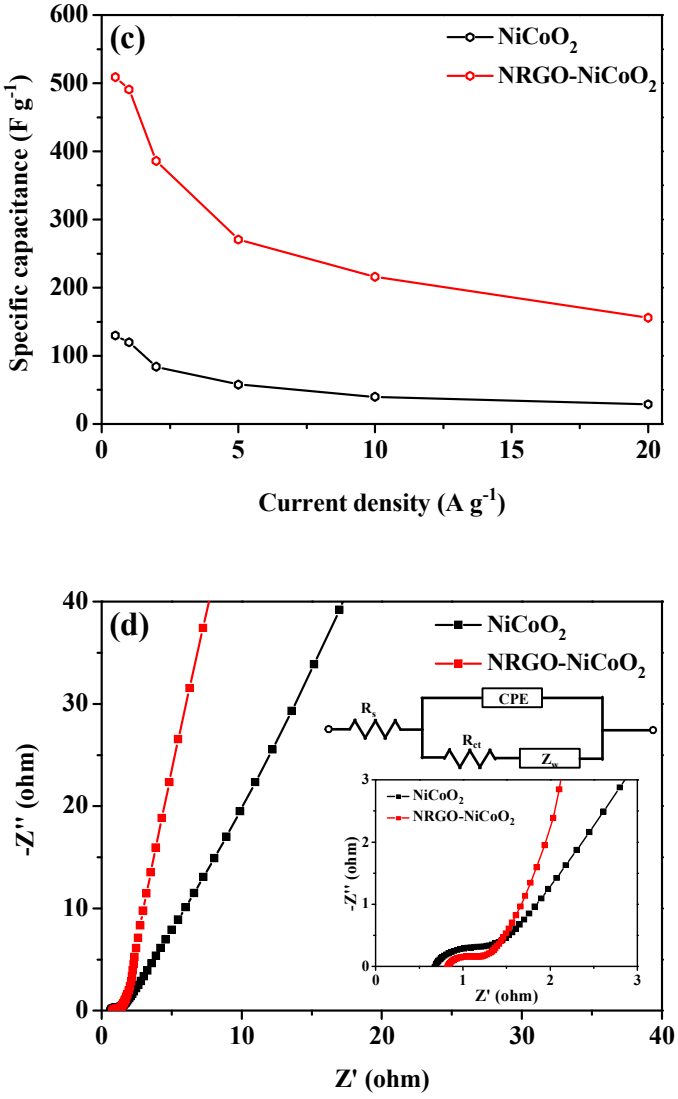


**Figure 4.** Electrochemical performance of pure $NiCoO_2$ nanoparticles and NRGO-$NiCoO_2$ composites prepared from 54 wt.% urea addition: (a) CV curves of pure $NiCoO_2$ nanoparticles and NRGO-$NiCoO_2$ composites at a scan rage of 50 mV $s^{-1}$, (b) galvanostatic charge-discharge curves of pure $NiCoO_2$ nanoparticles and NRGO-$NiCoO_2$ composites at the current density of 1 A $g^{-1}$, (c) specific capacitance of pure $NiCoO_2$ nanoparticles and NRGO-$NiCoO_2$ composites at various current density from 0.5 A $g^{-1}$ to 20 A $g^{-1}$, (d) EIS curves of $NiCoO_2$ nanoparticles and NRGO-$NiCoO_2$ composites.

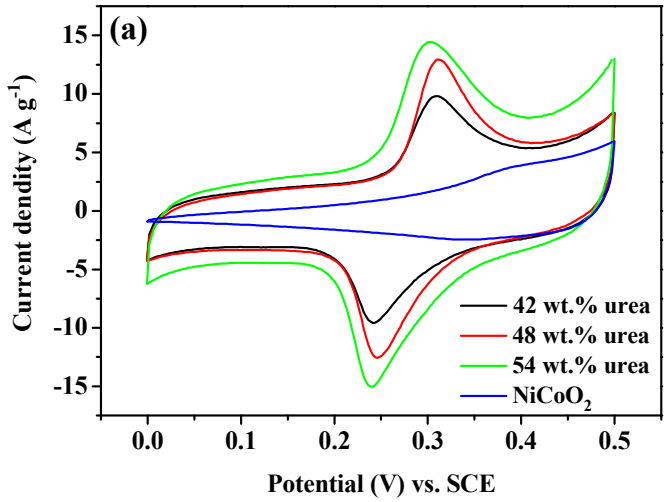


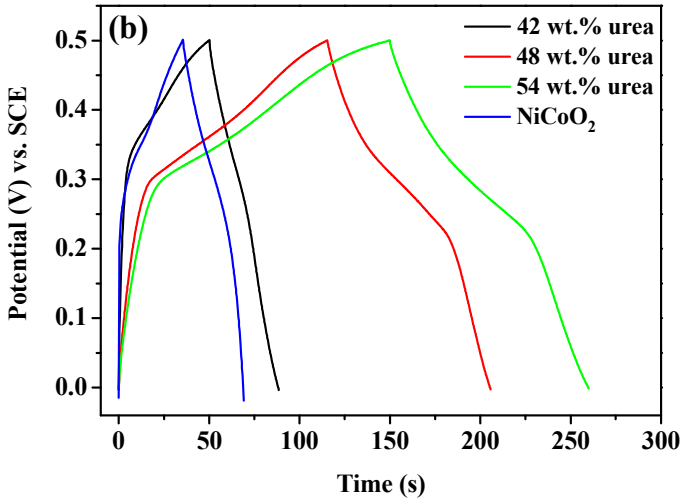

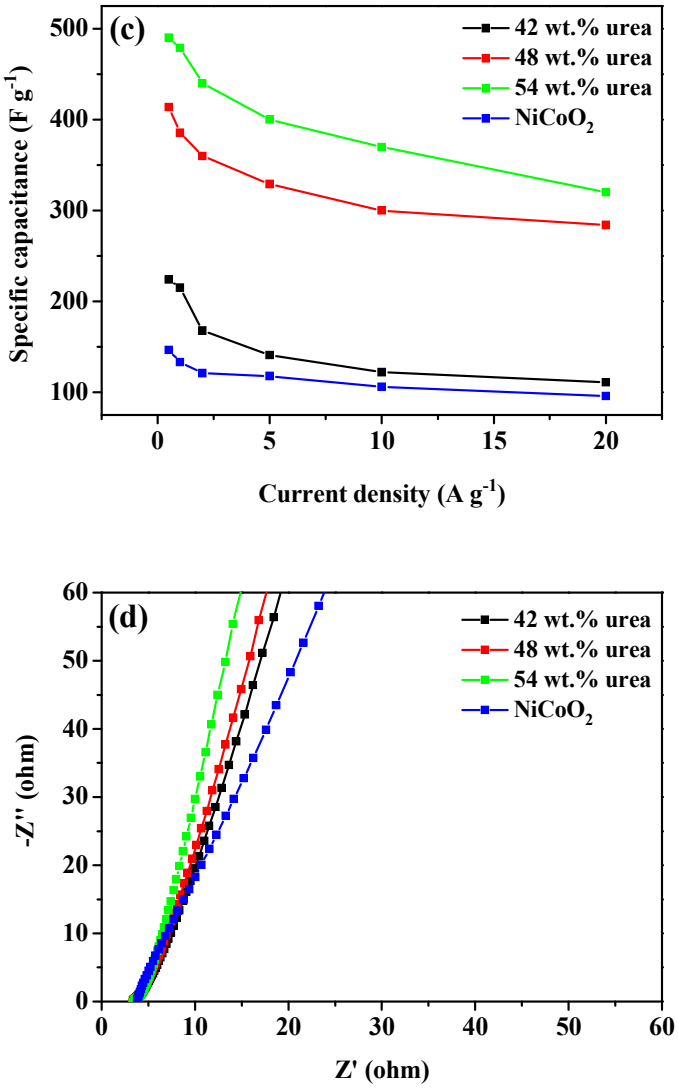


**Figure 5.** Electrochemical performance of NRGO-$NiCoO_2$ composites with increasing weight rate of urea: (a) CV curves at a scan rate of 20 mV $s^{-1}$, (b) GCD curves at a current density of 1 A $g^{-1}$, (c) specific capacitance at various current density from 0.5 A $g^{-1}$ to 20 A $g^{-1}$, (d) EIS curves of NRGO-$NiCoO_2$ composites.

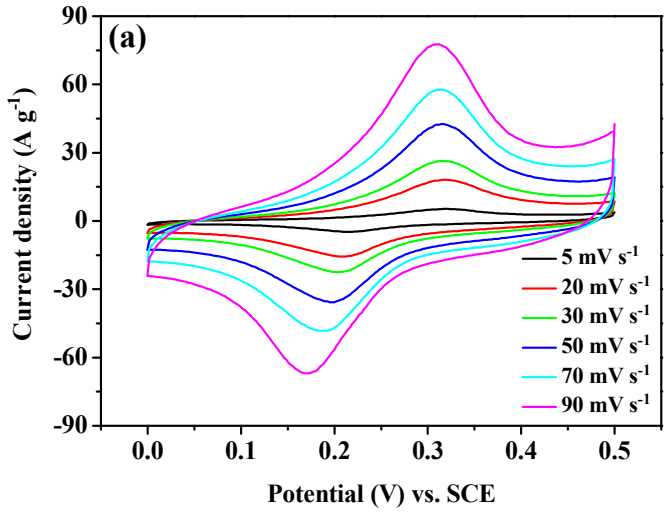


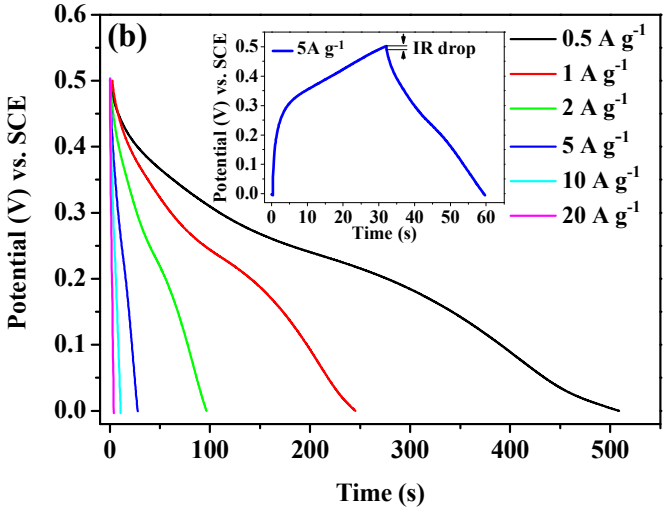

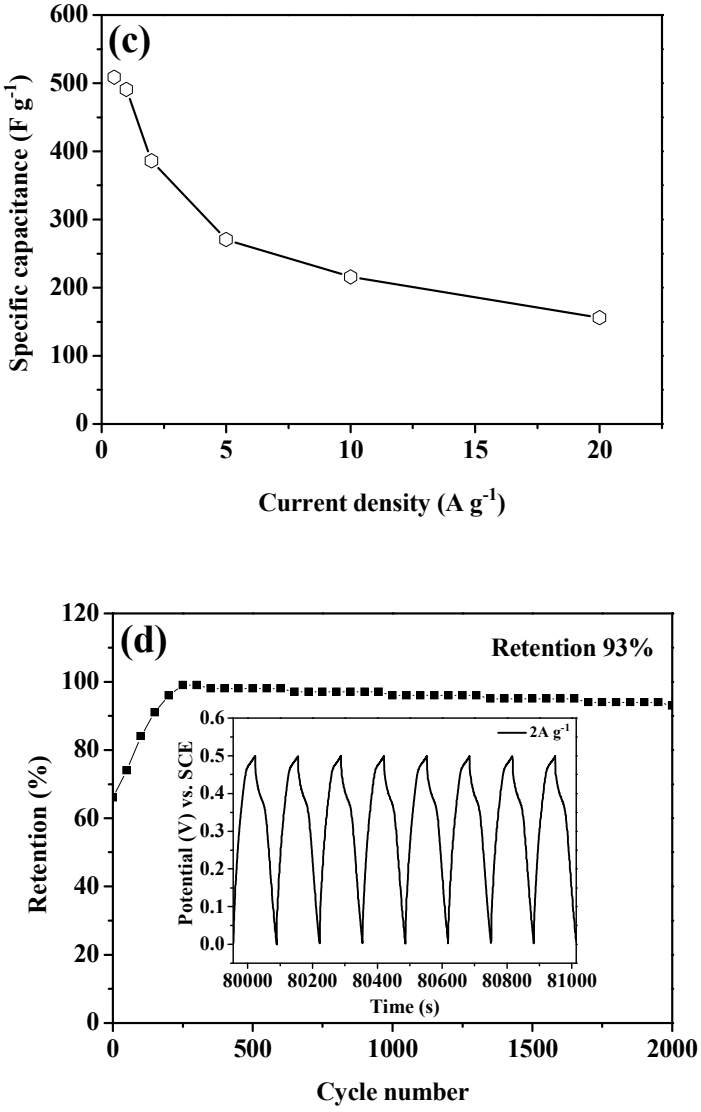


**Figure 6.** (a) Electrochemical performance of NRGO-$NiCoO_2$ composite materials: CV curves at various scan rates ranging from 5 to 90 mV $s^{-1}$, (b) galvanostatic discharge curves of the NRGO-$NiCoO_2$ composites at various currents densities from 0.5 A $g^{-1}$ to 20 A $g^{-1}$ and the typical galvanostatic charge-discharge curves at the current density of 5 A $g^{-1}$ in the inset of (b), (c) specific capacitance at various current density from 0.5 A $g^{-1}$ to 20 A $g^{-1}$, (d) cycle performance at current density of 2 A $g^{-1}$ and 8 galvanostatic charge-discharge curves at current density of 2 A $g^{-1}$ from 80000 sec. to 81000 sec. in the inset of (d).

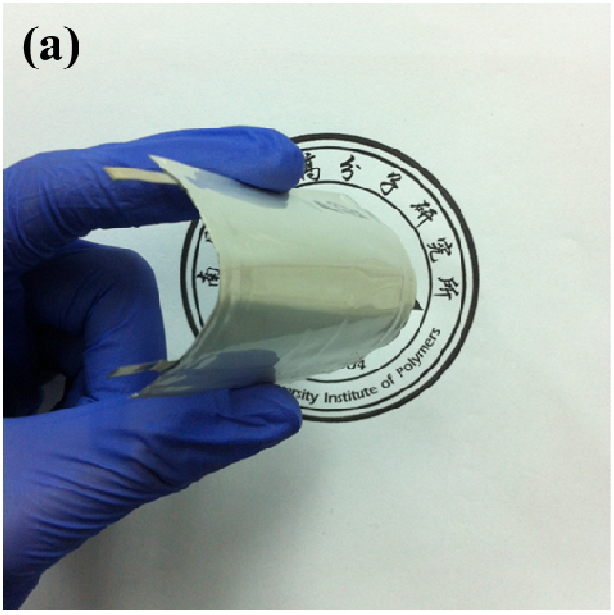


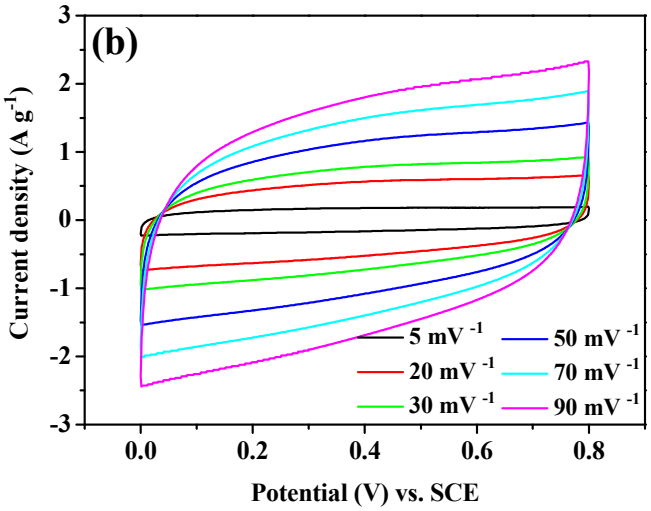

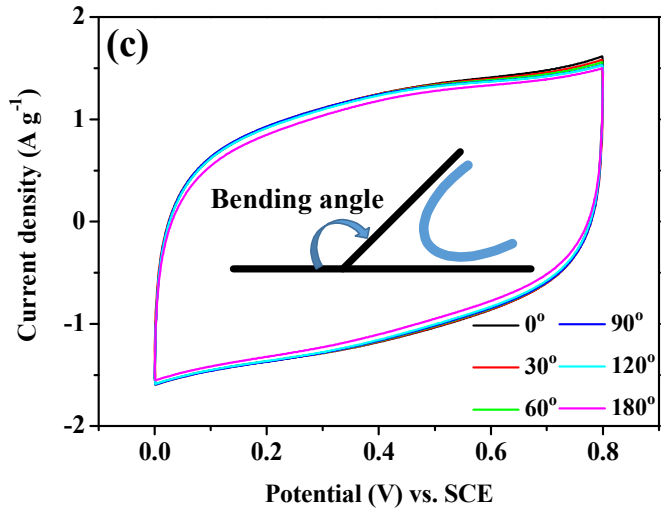


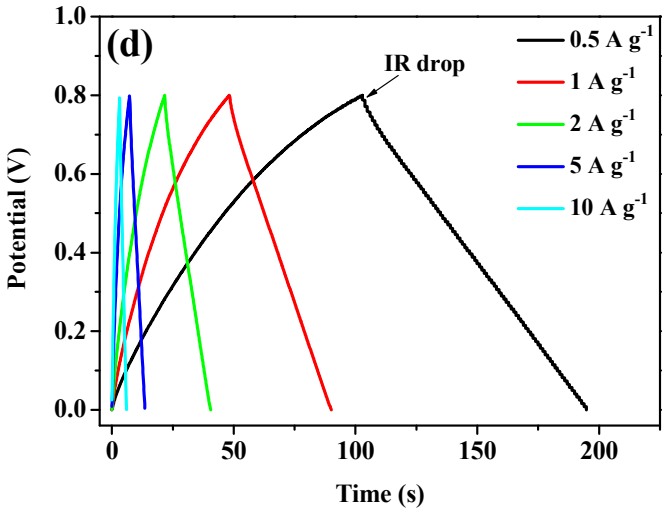

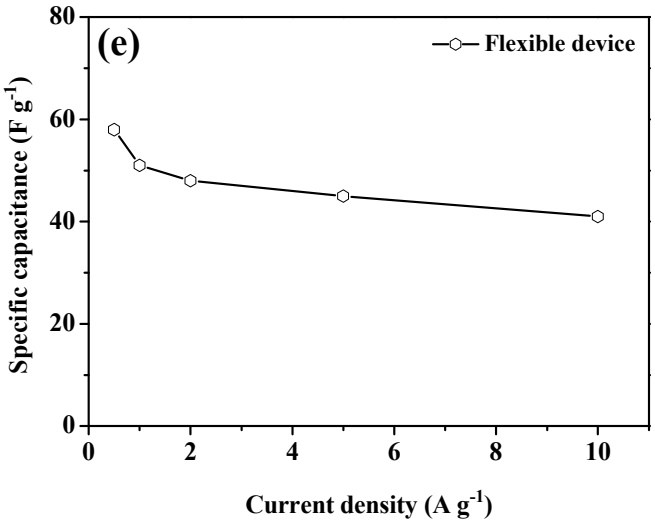


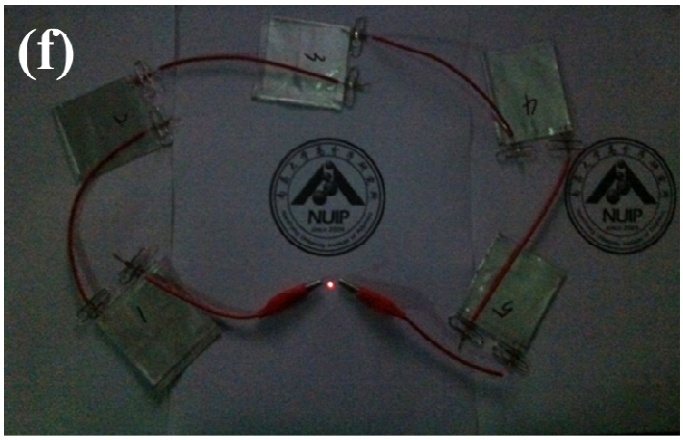


**Figure 7.** (a) The photograph of flexible devices, (b) CV curve of flexible devices at various scan rate ranging from 5 to 90 mV $s^{-1}$, (c) CV curve of flexible devices at various bending angle ranging from $0^{o}$ to $180^{o}$, (d) galvanostatic charge-discharge curves of flexible devices at various current density from 0.5 A $g^{-1}$ to 10 A $g^{-1}$, (e) specific capacitance at various current density from 0.5 A $g^{-1}$ to 10 A $g^{-1}$, (f) the photograph of demonstrate that a red light-emitting diode (LED) were light by the flexible devices.

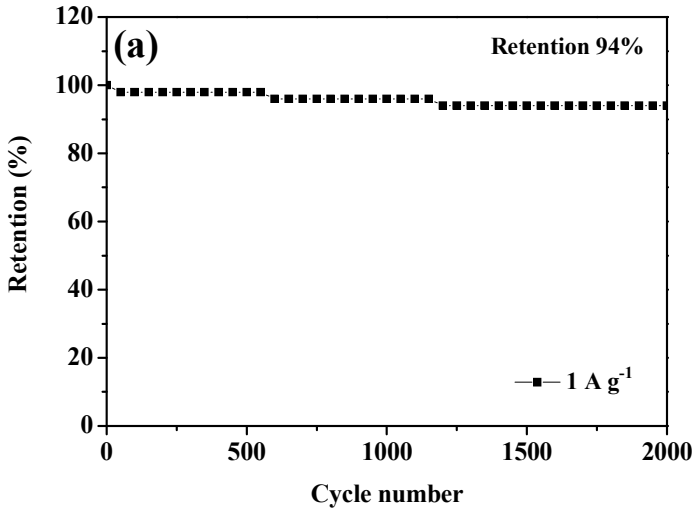


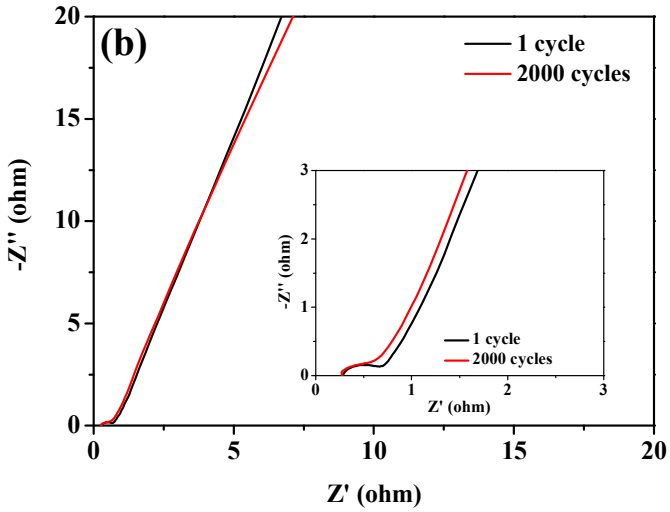

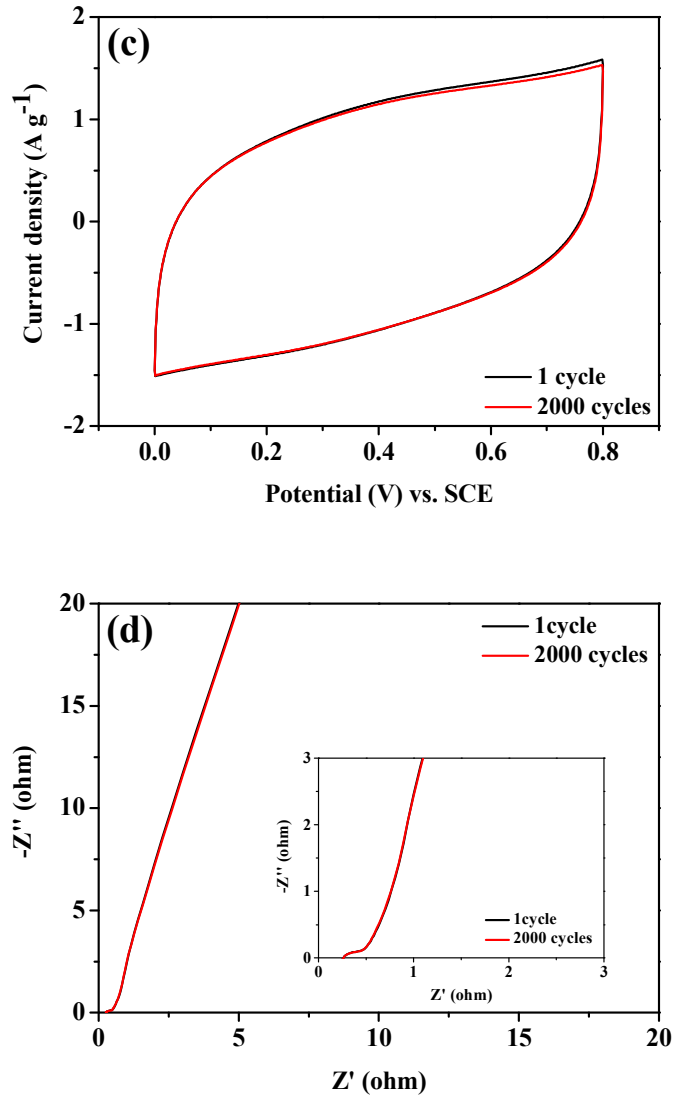


**Figure 8.** (a) Cycle performance of flexible devices at current density of 1 A $g^{-1}$ by GCD test, (b) EIS curves of flexible devices before and after 2000 cycles by GCD test, (c) cycle performance of flexible devices at the scan rate of 50 mV $s^{-1}$, (d) EIS curves of flexible devices before and after 2000 cycles by CV test.

## Highlights

**A Facile Approach to $NiCoO_2$ Intimately Standing on Nitrogen Doped Graphene Sheets by One-step hydrothermal Synthesis for Supercapacitors**

Yazhou Xu, Junchao Wei, Licheng Tan, Ji Yu, Yiwang Chen*

The binary nickel cobaltite oxides intimately standing on nitrogen doped reduced graphene sheets are prepared utilizing a one-step hydrothermal synthesis.

## Graphic abstract